ACCELERATING REDUNDANT DCT FILTERING FOR DEBLURRING AND DENOISING

Norishige Fukushima, Yuki Kawasaki, and Yoshihiro Maeda

Nagoya Institute of Technology, Japan

ABSTRACT

In this paper, we propose an acceleration method of redundant DCT filtering for deblurring and denoising. Current CCD cameras have high-resolution images, and the resolution has been increasing. Even if pixels are in focus, the pixels have slight blurring due to diffraction and Bayer interpolation. Therefore, we focus deblurring for slight blurring on real-time performance. Traditional approaches have a fast computational performance for this purpose, but these methods do not contain denoising architecture. In this paper, we simultaneously perform deblurring and denoising on the redundant DCT domain for accelerating the process. Also, we show that a post-scaling DCT can accelerate the proposed filtering. Experimental results show that the proposed method is the fastest method and the accuracy is also high among the fast approaches.

***Index Terms*—** DCT deblurring, redundant DCT filtering, post-scale DCT, acceleration

1. INTRODUCTION

Current CCD cameras have high-resolution images, and the resolution has been increasing. The CCD becomes smaller and smaller; thus, diffraction is inevitable. The diffraction generates small blurring for images. Also, Bayer interpolation slightly blurs images. Therefore deblurring is essential in image processing [1].

State-of-the-arts deblurring can adopt complex and large blurring kernels; however, the computational cost of these processes tends to be high. In this paper, we will deconvolve small blurred images; hence, these methods are overabundance tolerance for complex problems. Even traditional approaches, such as Lucy-Richardson's deconvolution [2, 3], iterative back projection [4], and Wiener deconvolution in frequency domain [5] can recover the problem with low cost.

Spatial domain approaches deconvolve an image at high speed for the small blurred images. These filters are the Lucy-Richardson's deconvolution and iterative back projection. The methods require iterative filtering. For large images, the iteration is not suitable since computed results are not on cache memories. Frequency domain filtering recovers images with one iteration; however, ringing artifacts are inevitable. Moreover, these approaches do not have denoising functionality. These approaches require denoising as preprocessing.

Fast Fourier transformation (FFT) for the frequency domain filtering requires $O(S\log(S))$, where S is image size. The computational cost of FFT is high for large size images. Redundant DCT denoising [6] accelerates the frequency domain filtering by using small DCT patches. The filter requires multiple times of DCT, i.e., the number of image pixels; however, the transformation size is small. Therefore, the process tends to have smaller costs than the full-size transformation. The redundant processing also reduces ringing artifacts, which are natively caused by frequency domain filtering. Moreover, our previous work [7] accelerates the redundant DCT filtering, but the filter focuses on denoising.

In this paper, we proposed an acceleration of the redundant DCT filtering for simultaneously deblurring and denoising. We adopt deconvolution in the frequency domain of redundant DCT processing. We also extend a fast DCT algorithm of Arai-Agui-Nakajima (AAN) [8], which is a post-scaling DCT and used in JPEG, for the redundant DCT filtering. The contributions of this paper are as follows:

- We proposed a fast DCT filter for simultaneously deblurring and denoising with redundant DCT filtering.
- We accelerate the DCT deblurring by a post-scale DCT.

2. RELATED WORK

When a blurring kernel is known, the deconvolution problem is called *non-blind deconvolution*. We review the non-blind deconvolution in the spatial and frequency domain. Lucy-Richardson's deconvolution (LR) [2, 3] utilizes spatial domain filtering for deblurring with iterative filtering. Iterative back projection (IBP) [4] extends the Lucy-Richardson's work to utilize a back projection kernel. IBP is the same as LR deconvolution when the back projection kernel and the blurring kernel are identity, and a step parameter in the steeped descent algorithm is 1. Bilateral back projection [9] uses bilateral filtering [10] for the back projection kernel. The bilateral filtering is also utilized in LR deconvolution [11]. Non-local back projection [12] utilizes non-local means filtering [13] for the kernel. Adjusting the minimization method can accelerate the iterative processing [14, 15]. The back-projection-based

This work was supported by JSPS KAKENHI (JP17H01764, JP18K19813).

 © IEEE 2019

approaches do not involve regularization function; thus, these methods suffer from image noises. For noisy images, these approaches require an additional process of denoising.

Frequency domain approaches utilize FFT for deblurring. Without a regularization function or with a Gaussian prior, they have a closed-form solution [16]. We can solve the problem by FFT without iteration. Iterative processing is required only for using better prior, such as natural image prior [16] and hyper-Laplacian prior [17], since the solutions require a non-convex optimization. For each processing, we perform multiple times of FFT. The FFT based approaches are fast and robust for large blurring kernel. However, in the case of the slightly blurring case, back-projection-based approaches are fast, since FFT depends on image size.

For accelerating the frequency domain filter, redundant DCT filtering with small DCT patches is proposed [6]. The redundant DCT filter also suppress ringing. BM3D filtering [18] utilizes the redundant frequency filtering for the 3D domain to improve the accuracy. The our previous works accelerate the DCT filtering [7, 19].

3. DCT DENOISING

3.1. Algorithm

The redundant DCT denoising generates a patch per a pixel and transforms the patch to DCT domain [6]. The processing patch is sliding to the next pixel. First, the i-th patch p_i in an image is transformed into the DCT domain:

$$P_i = \mathcal{C}(p_i), \tag{1}$$

where P_i is coefficients of p_i. $\mathcal{C}(\cdot)$ is a DCT function. Next, the noisy coefficients set to zero by hard-thresholding:

$$P'_i(u,v) = \begin{cases} P_i(u,v) & u = v = 0 \\ P_i(u,v) & |P_i(u,v)| > T \\ 0 & otherwise. \end{cases} \tag{2}$$

P'_i is coefficients after thresholding. T is the threshold value. $|\cdot|$ indicates a absolute difference operator. u and v are patch coordinates. Notice that we do not perform thresholding for the direct current (DC) component to keep bias. Finally, inverse DCT of $\mathcal{C}^{-1}$ transforms P'_i into the spatial domain:

$$p'_i = \mathcal{C}^{-1}(P'_i), \tag{3}$$

where p'_i is a denoised patch in the spatial domain. We perform the DCT filtering for each patch in an image. After patch filtering, we average all patches to obtain the result:

$$J(\boldsymbol{x}) = \frac{1}{|\omega(\boldsymbol{x})|} \sum_{\boldsymbol{y} \in \omega(\boldsymbol{x})} p'_{\boldsymbol{y}}, \tag{4}$$

where $J(\boldsymbol{x})$ is an output on a pixel $\boldsymbol{x}$. $\omega(\boldsymbol{x})$ is a set of patch-indexes around $\boldsymbol{x}$ $|\omega(\boldsymbol{x})|$ is the number of patches in the set.

For RGB images, we use 3-point DCT to remove color correlations, and then we perform the redundant DCT denoising for each channel. The orthonormal basis is defined by:

$$\left\{ \left(\frac{1}{\sqrt{3}}, \frac{1}{\sqrt{3}}, \frac{1}{\sqrt{3}}\right)^T, \left(\frac{1}{\sqrt{2}}, 0, -\frac{1}{\sqrt{2}}\right)^T, \left(\frac{1}{\sqrt{6}}, -\frac{2}{\sqrt{6}}, \frac{1}{\sqrt{6}}\right)^T \right\} \tag{5}$$

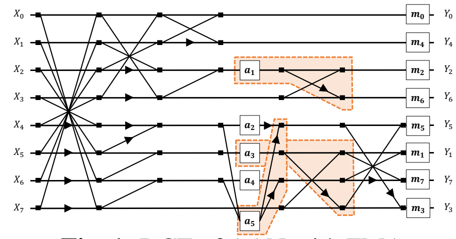

Fig. 1: DCT of AAN with FMA.

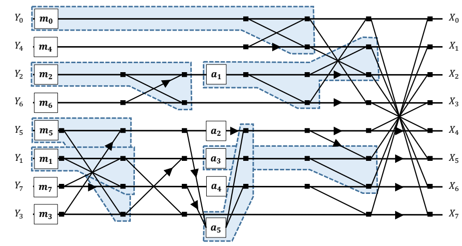

Fig. 2: Inverse DCT of AAN with FMA.

The decorrelation can improve the denoising performance than a standard color transformation, such as the YUV and Lab color space.

3.2. Acceleration of DCT Denoising

Our previous work accelerates the DCT denoising with the fast 8-point DCT [7]. Loeffler-Ligtenberg-Moschytz (LLM) [20] and AAN are fast DCT methods, and JPEG utilizes both approaches. The post scaling DCT of AAN is suitable for the redundant DCT filtering.

In AAN, scaling adjustment is located in post-processing of DCT and pre-processing of IDCT. Figures 1 and 2 show the diagrams of DCT and IDCT. The processes have the smaller number of additions and multiplications than the usual DCT. Also, the DCT is accelerated by the fused-multiply-add (FMA) intrinsic on the hardware accelerator. The colored region indicates arithmetic operations with FMA. The post-processing of the scaling operators is merged with that of multiplications in pre-processing. Moreover, the merged processing is joined with the hard-thresholding in DCT denoising (See Fig. 3). For the thresholding, we only perform scaling for a scaled thresholding map. Instead of using Eq. (2) of T, we use the scaled thresholding map $\tau(u,v)$.

$$\tau(u,v) = \frac{T}{m_u \times m_v}, \tag{6}$$

where m_u and m_v are horizontal and vertical scaling values for 1D-DCT, respectively. The i-th patch filtering for the DCT coefficients are as follows:

$$P'_i(u,v) = \begin{cases} P_i(u,v) \circ M(u,v) & u = v = 0 \\ P_i(u,v) \circ M(u,v) & |P_i(u,v)| > \tau(u,v) \\ 0 & otherwise, \end{cases} \tag{7}$$

where $M(u,v)$ is a scaling map for 2D DCT. The operator of $\circ$ represents an element-wise product of matrices. By this ac-

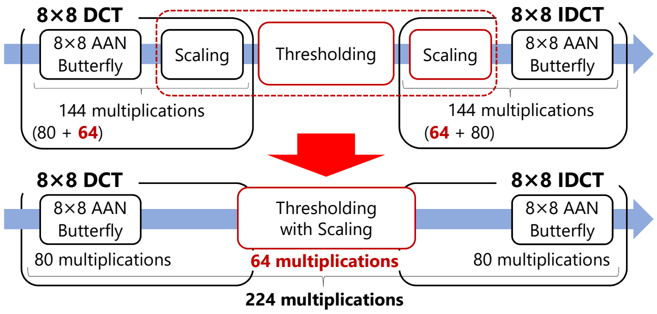

Fig. 3: DCT filtering with post scaling DCT of AAN.

celeration, the total number of multiplications decreases from 288 to 224, and also that of data accessing decreases. FMA further accelerates the DCT denoising.

4. PROPOSED METHOD

4.1. Redundant DCT Deblurring

Convolution of linear filters is represented by a element-wise multiplication in the frequency domain. A division of a blurring function represents deconvolution. Frequency domain deblurring in the DCT domain is defined by:

$$J = \mathcal{C}^{-1}\Big(\frac{\mathcal{C}(I)}{\max(\mathcal{C}(g), \epsilon)}\Big), \tag{8}$$

where I and J are input and output images, respectively. g is the Gaussian kernel. ϵ is a small value for preventing zero division. The Gaussian function is as follows:

$$g(s,t) = \exp\Big(-\frac{s^2+t^2}{2\sigma^2}\Big), \tag{9}$$

where σ is a smoothing parameter, and s and t are image coordinates in the spatial domain, respectively.

Transforming the representation (8) into redundant DCT filtering, we apply the DCT domain filtering to a image patch:

$$p'_i = \mathcal{C}^{-1}\Big(\frac{\mathcal{C}(p_i)}{\max(\mathcal{C}(g), \epsilon)}\Big). \tag{10}$$

After per-patch processing, we average the patches.

$$J(\boldsymbol{x}) = \frac{1}{|\omega(\boldsymbol{x})|}\sum_{y\in\omega(\boldsymbol{x})} p'_y, \tag{11}$$

There are several types of DCT [21]. For DCT denoising, DCT-II is utilized. However, the Gaussian function is a symmetric function at $(m,n) = (0,0)$; hence, DCT-II cannot convert the kernel well due to boundary conditions. In this paper, we use DCT-I for the transform to solve the problem.

4.2. Redundant DCT Deblurring and Denoising

This section describes the simultaneous processing of deblurring and denoising. We can realize the processing by both thresholding and division for DCT coefficients in redundant filtering. The filtering for the i-th patch is represented by:

$$P'_i(u,v) = \begin{cases} \frac{P_i(u,v)}{\max(G(u,v),\epsilon)} & u=v=0 \\ \frac{P_i(u,v)}{\max(G(u,v),\epsilon)} & |P_i(u,v)| > T \\ 0 & otherwise, \end{cases} \tag{12}$$

where, G is coefficients of DCT for the deblurring Gaussian function. P'_i is DCT coefficients of the deblurred and denoised patch. The patch is transformed into the spatial domain by Eq. (3). The DCT filtering is performed for each pixel. Finally, the processed patched are averaged by Eq. (11).

4.3. Acceleration by Post-scaling DCT

We can also accelerate the DCT deblurring and denoising by using the post-scaling DCT of AAN. The filtering with AAN for the i-th patch is represented by:

$$P'_i(u,v) = \begin{cases} \frac{P_i(u,v)\circ M(u,v)}{\max(G(u,v),\epsilon)} & u=v=0 \\ \frac{P_i(u,v)\circ M(u,v)}{\max(G(u,v),\epsilon)} & |P_i(u,v)| > \tau(u,v) \\ 0 & otherwise. \end{cases} \tag{13}$$

The elements in the matrix $\frac{M(u,v)}{\max(G(u,v),\epsilon)}$ is constant for each patches; thus, we can use precomputed values for matrix arithmetic operations.

$$P'_i(u,v) = \begin{cases} P_i(u,v)\circ N(u,v) & u=v=0 \\ P_i(u,v)\circ N(u,v) & |P_i(u,v)| > \tau(u,v) \\ 0 & otherwise, \end{cases} \tag{14}$$

where $N(u,v) = \frac{M(u,v)}{\max(G(u,v),\epsilon)}$. The representation (14) is the same as Eq. (7), the computational time of the DCT denoising and deblurring is the same as the DCT denoising only.

5. EXPERIMENTAL RESULTS

We verified the proposed method by the computational cost and accuracy. We compared our method with the iterative back projection (IBP) [4], bilateral back projection (BBP) [9] and DCT domain filtering without redundant processing on full image size (F-DCT) (Eq. (8)). IBP and BBP do not have denoising structure; thus, we performed DCT denoising as preprocessing. The DCT denoising has higher denoising performance than the simple bilateral filtering [10]. The computational cost of DCT denoising is faster than the bilateral filtering even using the optimized code [22, 23]. Note that we terminated the number of iterations until 10 for acceleration in IBP and BBP. We wrote the code by C++ optimized by AVX/AVX2 and parallelized by OpenMP. We compiled the program by VisualStudio 2017. In the back projection approaches, there are several accelerations for Gaussian filtering. The Gaussian filter can be accelerated by FIR separable filtering [24] or recursive filtering [25].

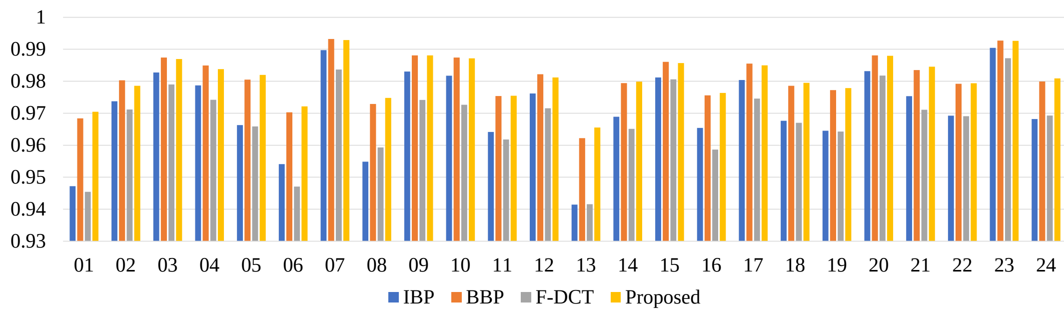

Fig. 4: MS-SSIM score of each method in Kodak 24 images.

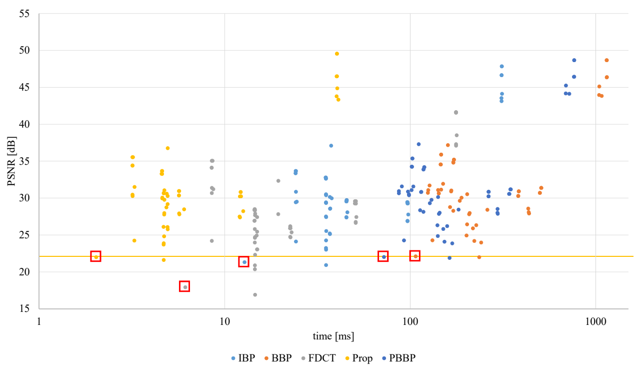

Fig. 5: PSNR and computational time for various image dataset (the resolution is from 512×512 to 2264×1512) and various degrading parameters $\sigma_n = \{0.0, 1.0, 2.0\}$ and $\sigma_b = \{1.5, 2.0, 2.5, 3.0\}$, where σ_n and σ_b are parameters of additive white noises and Gaussian distribution for blurring. Red rectangles indicate the same condition (image and degrading parameters) for each method.

Table 1: Computational time of each method [ms].

	IBP	BBP	F-DCT	Prop.	P-BBP
time	27.08	127.36	13.14	**8.38**	108.50

For accuracy evaluation, we use two metrics; PSNR and MS-SSIM [26], which is an extention of SSIM [27]. MS-SSIM has high correlation to the human visual sense of deblurred images [28]. Test data are USC-SIPI Image Database and Kodak 24 image dataset.

Figure 4 shows the accuracy score of MS-SSIM for each image in Kodak dataset (768×512). Table 1 shows the computational time. BBP has the slightly higher accuracy score than the proposed method, but its computational cost is $\times 10$ slower than the proposed method. Notice that we can use the proposed method for the initial estimation of the bilateral back filtering. The initialization reduces the number of iterations. P-BBP means that the proposed method utilized for the initialization of BBP. P-BBP can reduce the number of iterations from 10 to 7 whilst keeping the accuracy. Therefore, we can also improve the computational performance for iterative spatial domain filtering. In BBP, we use OpenCV's implementation of bilateral filtering. The acceleration methods of bilateral filtering [29, 30] can improve the performance.

Fig. 6: Input and results: input image, IBP, and proposed result from left to right, respectively.

Figure 5 shows the scatter plot of the computational time and PSNR of each method for various image dataset with various parameters. The plots indicate that left-top points have high performance. The proposed method has the highest speed among them. Also the proposed method is higher accuracy than IBP and the almost the same quality in PSNR for the other method. Note that horizontal axis is log scale; thus, the proposed method is quat fast.

Figure 6 depicts deblurring results of a real image. The proposed method can recover the sharp edge and texture.

6. CONCLUSION

In this paper, we focused on the small blurring and weak noise recovery problem. We proposed the redundant DCT filtering for simultaneous processing of deblurring and denoising for efficient computation. The filter utilizes redundant DCT filtering for acceleration and suppressing ringing effect. We also proposed an acceleration technique for the extended redundant DCT filtering by using the post scaling DCT. The experimental results showed that the proposed method has the highest computational performance and recovering accuracy among the iterative back projection and simple frequency domain filtering, which are known as efficient methods.

7. REFERENCES

[1] P. C. Hansen, J. G. Nagy, and D. P. O'leary, *Deblurring images: matrices, spectra, and filtering*, vol. 3, SIAM, 2006.

[2] W. H. Richardson, "Bayesian-based iterative method of image restoration," *Journal of the Optical Society of America*, vol. 62, no. 1, pp. 55–59, 1972.

[3] L. B. Lucy, "An iterative technique for the rectification of observed distributions," *The Astronomical Journal*, vol. 79, pp. 745, 1974.

[4] M. Irani and S. Peleg, "Improving resolution by image registration," *Graphical Models and Image Processing (CVGIP)*, vol. 53, no. 3, pp. 231–239, 1991.

[5] N. Wiener, *Extrapolation, interpolation, and smoothing of stationary time series*, The MIT Press, 1964.

[6] G. Yu and G. Sapiro, "Dct image denoising: A simple and effective image denoising algorithm," *Image Processing On Line*, vol. 1, pp. 1, 2011.

[7] Y. Kawasaki, Y. Maeda, and N. Fukushima, "Parallelized and vectorized implementation of dct denoising with fma instructions," in *Proc. International Workshop on Advanced Image Technology (IWAIT)*, 2018.

[8] Y. Arai, T. Agui, and M. Nakajima, "A fast dct-sq scheme for images," *IEICE Transactions*, vol. E-71, no. 11, pp. 1095–1097, 1988.

[9] S. Dai, M. Han, Y. Wu, and Y. Gong, "Bilateral back-projection for single image super resolution," in *Proc. IEEE International Conference on Multimedia and Expo (ICME)*, 2007.

[10] C. Tomasi and R. Manduchi, "Bilateral filtering for gray and color images," in *Proc. IEEE International Conference on Computer Vision (ICCV)*, 1998.

[11] L. Yuan, J. Sun, L. Quan, and H.-Y. Shum, "Progressive interscale and intra-scale non-blind image deconvolution," *ACM Transactions on Graphics*, vol. 27, no. 3, 2008.

[12] W. Dong, L. Zhang, G. Shi, and X. Wu, "Nonlocal back-projection for adaptive image enlargement," in *Proc. IEEE International Conference on Image Processing (ICIP)*, 2009.

[13] A. Buades, B. Coll, and J. M. Morel, "A non-local algorithm for image denoising," in *Proc. IEEE Conference on Computer Vision and Pattern Recognition (CVPR)*, 2005.

[14] M. K. Singh, U. S. Tiwary, and Y.-H. Kim, "An adaptively accelerated lucy-richardson method for image deblurring," *EURASIP Journal on Advances in Signal Processing*, 2008.

[15] H. Wang and P. C. Miller, "Scaled heavy-ball acceleration of the richardson-lucy algorithm for 3d microscopy image restoration," *IEEE Transactions on Image Processing*, vol. 23, no. 2, pp. 848–854, 2014.

[16] A. Levin, R. Fergus, F. Durand, and W. T. Freeman, "Image and depth from a conventional camera with a coded aperture," *ACM Transactions on Graphics*, vol. 26, no. 3, 2007.

[17] D. Krishnan and R. Fergus, "Fast image deconvolution using hyper-laplacian priors," in *Proc. Advances in Neural Information Processing Systems (NIPS)*, 2009.

[18] K. Dabov, A. Foi, V. Katkovnik, and K. Egiazarian, "Image denoising by sparse 3-d transform-domain collaborative filtering," *IEEE Transactions on Image Processing*, vol. 16, no. 8, pp. 2080–2095, 2007.

[19] S. Fujita, N. Fukushima, M. Kimura, and Y. Ishibashi, "Randomized redundant dct: Efficient denoising by using random subsampling of dct patches," in *Proc. SIGGRAPH Asia, Technical Briefs*, 2015.

[20] C. Loeffler, A. Ligtenberg, and G. S. Moschytz, "Practical fast 1-d dct algorithms with 11 multiplications," in *Proc. IEEE International Conference on Acoustics, Speech and Signal Processing (ICASSP)*, 1989.

[21] N. Ahmed, T. Natarajan, and K. R. Rao, "Discrete cosine transform," *IEEE Transactions on Computers*, vol. 100, no. 1, pp. 90–93, 1974.

[22] Y. Maeda, N. Fukushima, and H. Matsuo, "Taxonomy of vectorization patterns of programming for fir image filters using kernel subsampling and new one," *Applied Sciences*, vol. 8, no. 8, 2018.

[23] Y. Maeda, N. Fukushima, and H. Matsuo, "Effective implementation of edge-preserving filtering on cpu microarchitectures," *Applied Sciences*, vol. 8, no. 10, 2018.

[24] N. Fukushima, Y. Maeda, Y. Kawasaki, M. Nakamura, T. Tsumura, K. Sugimoto, and S. Kamata, "Efficient computational scheduling of box and gaussian fir filtering for cpu microarchitecture," in *Proc. Asia-Pacific Signal and Information Processing Association Annual Summit and Conference (APSIPA)*, 2018.

[25] K. Sugimoto, S. Kyochi, and S. Kamata, "Universal approach for dct-based constant-time gaussian filter with moment preservation," in *Proc. IEEE International Conference on Acoustics, Speech and Signal Processing (ICASSP)*, 2018.

[26] Z. Wang, E. P. Simoncelli, and A. C. Bovik, "Multiscale structural similarity for image quality assessment," in *Proc. Asilomar Conference on Signals, Systems Computers*, 2003.

[27] Z. Wang, A. C Bovik, H. R. Sheikh, and E. P. Simoncelli, "Image quality assessment: from error visibility to structural similarity," *IEEE Transactions on Image Processing*, vol. 13, no. 4, pp. 600–612, 2004.

[28] W.-S. Lai, J.-B. Huang, Z. Hu, N. Ahuja, and M.-H. Yang, "A comparative study for single image blind deblurring," in *Proc. IEEE Conference on Computer Vision and Pattern Recognition (CVPR)*, 2016.

[29] K. Sugimoto, N. Fukushima, and S. Kamata, "200 fps constant-time bilateral filter using svd and tiling strategy," in *Proc. IEEE International Conference on Image Processing (ICIP)*, 2019.

[30] N. Fukushima, T. Tsubokawa, and Y. Maeda, "Vector addressing for non-sequential sampling in fir image filtering," in *Proc. IEEE International Conference on Image Processing (ICIP)*, 2019.